

## ADVANCED NUMERICAL APPROACHES TO THE SEISMIC SOIL AND STRUCTURAL RESPONSE ANALYSES

Angelo AMOROSI<sup>1</sup> Daniela BOLDINI<sup>2</sup> and Annamaria DI LERNIA<sup>3</sup>

**Abstract:** A 3D non-linear finite element approach is developed to study the free-field seismic ground response and the soil-structure interaction (SSI) phenomena at the Lotung site (Taiwan) during the earthquake event occurred on May 20 1986. The site was extensively instrumented with down-hole and surface accelerometers, these latter located also on a 1/4-scale nuclear power plant containment structure. An advanced constitutive model is adopted for simulating the soil behaviour, while a linear visco-elastic behaviour is assumed for the structural model. Both the free-field and SSI analyses are carried out applying the EW horizontal component of the acceleration time history as recorded at the depth of 47 m b.g.l. The predicted ground response results are in fair agreement with the recorded motion at depth and at the surface. Also, the dynamic response of structure is well captured for this specific seismic event, thus confirming the validity of the numerical approach.

### Introduction

The dynamic response of a structure resting on a soft soil deposit is likely to be affected by the interaction with this latter, in terms of variation of oscillation period and damping ratio, as compared to the response of the same structure resting on a rigid base (Veletsos and Nair, 1975; Wolf, 1985). The soil-structure interaction (SSI) effects have traditionally been evaluated by the substructure method, which consists in separately estimating the kinematic and inertial interaction effects, implicitly assuming linearity in both soil and structure behaviour. Nevertheless, the non-linear soil behaviour should be taken into account to correctly estimate the ground response and the SSI effects, especially for strong motion earthquakes. This can be done by performing a complete dynamic analysis by means of the direct method, which consists in carrying out realistic non-linear analyses in the time domain including the entire soil-structure system (e.g. Kramer, 1996).

In this paper a 3D non-linear finite element model, set up adopting the code PLAXIS 3D (Brinkgreve et al., 2013), is used to back-analyse the seismic ground response and the SSI phenomena affecting a 1/4-scale nuclear power plant containment structure as recorded at the Lotung Large-Scale Seismic Test site during the May 20 1986 earthquake. The elasto-plastic hysteretic model "Hardening Soil model with Small-Strain Stiffness" (HSsmall) (Benz, 2006) is selected to describe the soil behaviour while a linear visco-elastic model is assumed for the structures. The 3D numerical analyses are performed applying the EW component of the acceleration time history as recorded at the base of a down-hole accelerometric array. Results of the non-linear analyses are compared to the in-situ recorded down-hole and surface motions and to the acceleration time histories monitored on the 1/4-scale containment structure.

### The Lotung case study

The Large-Scale Seismic Test (LSST) site was located in Lotung, a highly seismic region in the North-East of Taiwan. The LSST research project, led by the Electric Power Research Institute (EPRI) in co-operation with the Taiwan Power Company (TPC), consisted in studying the seismic ground response and the dynamic response of two small-scale (1/4-scale and 1/12-scale models) nuclear power plant containment structures.

---

<sup>1</sup> Professor, Technical University of Bari, Bari (Italy), [angelo.amorosi@poliba.it](mailto:angelo.amorosi@poliba.it)

<sup>2</sup> Professor, University of Bologna, Bologna (Italy), [daniela.boldini@unibo.it](mailto:daniela.boldini@unibo.it)

<sup>3</sup> PhD candidate, Technical University of Bari, Bari (Italy), [annamaria.dilernia@poliba.it](mailto:annamaria.dilernia@poliba.it)

The 1/4-scale model was a reinforced concrete cylindrical shell structure with a flat roof slab and a flat bottom basemat. Within the prototype model, a steel shell structure simulating a steam generator of a nuclear power plant was installed.

The LSST site was extensively instrumented to record both structural and soil response during earthquakes. Concerning the ground response instrumentation, surface arrays were installed along three arms (Arm 1, 2 and 3) of radius of about 47 m from the 1/4-scale model, while two down-hole instrument arrays, extended to a depth of 47 m from ground surface, were also included in the seismic monitoring scheme, as depicted in Figure 1.

Concerning the 1/4-scale model, four accelerometers were placed on the basemat of the containment structure and four at the top surface of the model, along EW and NS diametrical directions. In addition, two accelerometers were placed at the top and the bottom of the steam generator model. Figure 2 shows a sketch of the vertical and horizontal cross-sections of the 1/4-scale model (EPRI, 1991).

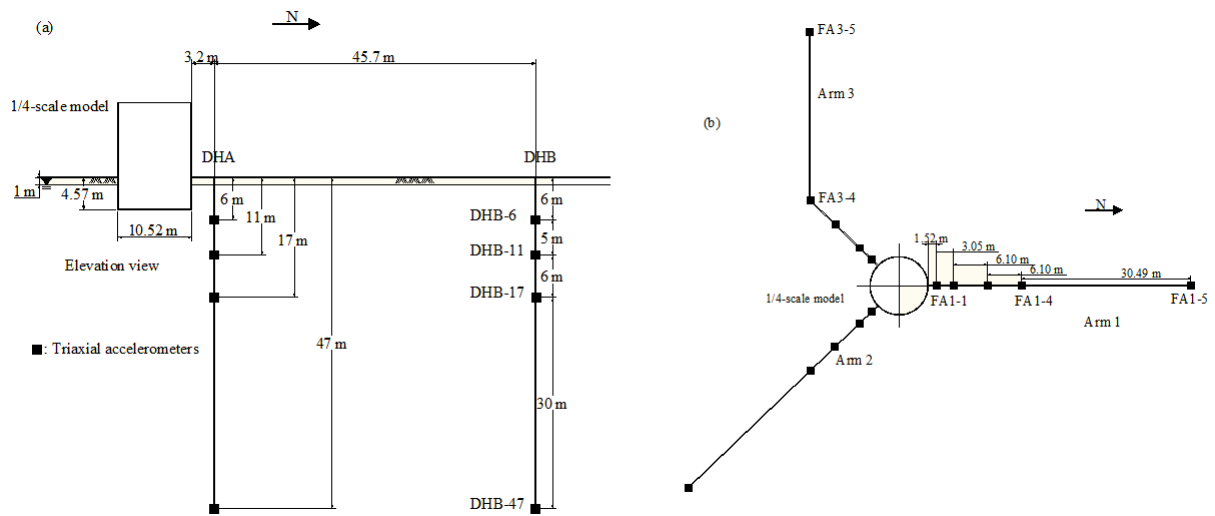


Figure 1. Location of surface and down-hole instrumentation: (a) elevation view and (b) plan view (modified from EPRI 1991).

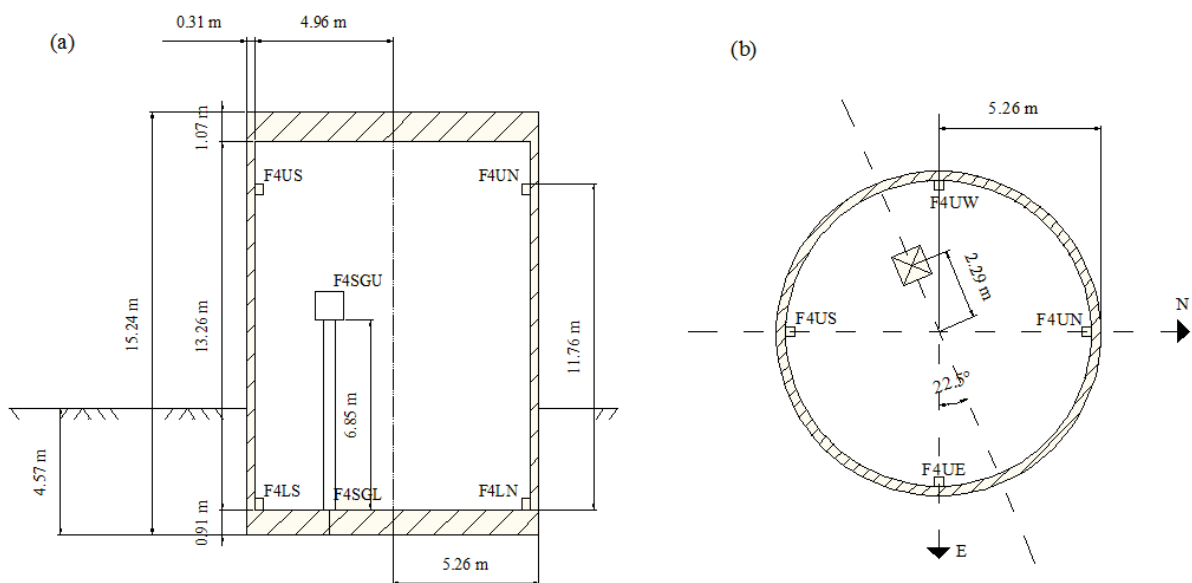


Figure 2. Locations of accelerometers on the 1/4-scale containment model: (a) vertical and (b) horizontal cross-section (modified from EPRI 1991).

The LSST site was located on the Lanyang River plain, which lies on two layers of recent alluvium and Pleistocene deposits, overlying a Miocene basement layer situated at 400 m of depth (EPRI, 1992). The local geotechnical profile, near the LSST site, is characterized by a layer of silty sand, extended from the ground surface down to about 17 m, above a 6 m thick layer of sand with gravel. This latter is resting on a stratum of silty clay detected by the deepest borehole down to 47 m, interlayered by an inclusion of sand with gravel between 29 m and 36 m. The water table is located at approximately 1 m from the ground surface (Figure 3a).

The geotechnical characterisation is based on the few available in situ data and on previously published back-analysed seismic data. In particular, the strength properties of the coarse-grained soils are obtained from SPT tests (Figure 3b), using the approach proposed by De Mellio (1971), while typical values were assumed for the silty clay layer, due to the lack of direct experimental observations. A total unit weight of 19.6 kN/m<sup>3</sup> is adopted as an average value for the whole soil deposit (Elgamal et al., 1995). The shear wave velocity profile was obtained from cross-hole tests, as depicted in Borja et al. (1999): it ranges from about 100 m/s to 300 m/s at a depth of 47 m (Figure 3c).

The assumed shear modulus and damping ratio curves for the upper silty sand layer are those obtained by Zeghal et al. (1995). Due to the lack of direct experimental data, these authors back-calculated the above dynamic properties at different depths, based on an indirect interpretation of 18 earthquakes events occurred between 1985 and 1986. The technique consisted in double integrating the recorded acceleration time histories to obtain the absolute displacements and then, by further differentiating them with respect to depth, determining the corresponding values of the shear strain. Assuming the one-dimensional shear beam idealisation, the shear stress was derived, based on a linear interpolation between down-hole accelerations. The estimated shear stress and strain seismic histories were thus used to evaluate the equivalent soil stiffness and damping ratio evolution with the strain level. For the finite element simulations, the shear modulus and damping ratio curves obtained at the depth of 11 m are assumed as representative of the average dynamic soil properties of the entire silty sand layer, as proposed by Borja et al. (2000).

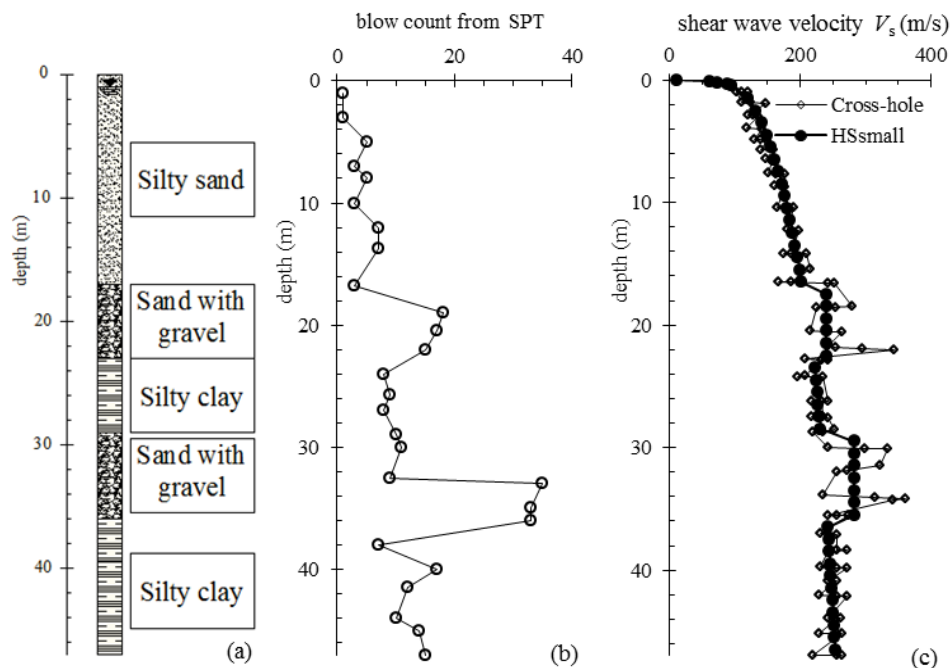


Figure 3. Soil profile at LSST site: (a) soil stratigraphy; (b) SPT log; (c) shear wave velocity.

Finally, due to the lack of specific laboratory tests, the shear modulus and damping ratio curves proposed by Vucetic and Dobry (1991) for a plasticity index PI equal to 0 and 20 are adopted for the gravelly and the silty-clayey layers, respectively (Figure 4).

In this paper the free-field seismic ground response and the dynamic structural response of the containment structure model are investigated with reference to the EW horizontal component of the acceleration time history recorded during the seismic event occurred on May 20 1986 (denoted as LLST7 and characterized by magnitude 6.5, epicentral distance of 66.2 km and duration of 35.48 s), as recorded at the depth of 47 m by the accelerometer DHB-47 (Figure 5).

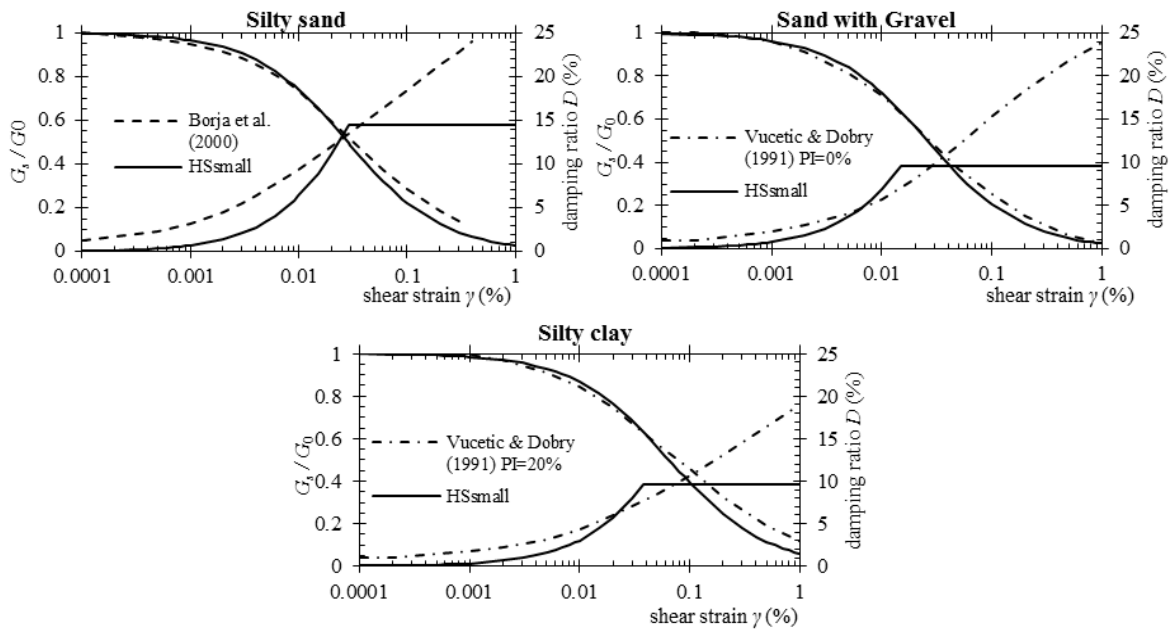


Figure 4. Shear stiffness modulus reduction curves and variation of damping ratio with shear strain assumed for the different soil layers and calibration of the HSsmall model.

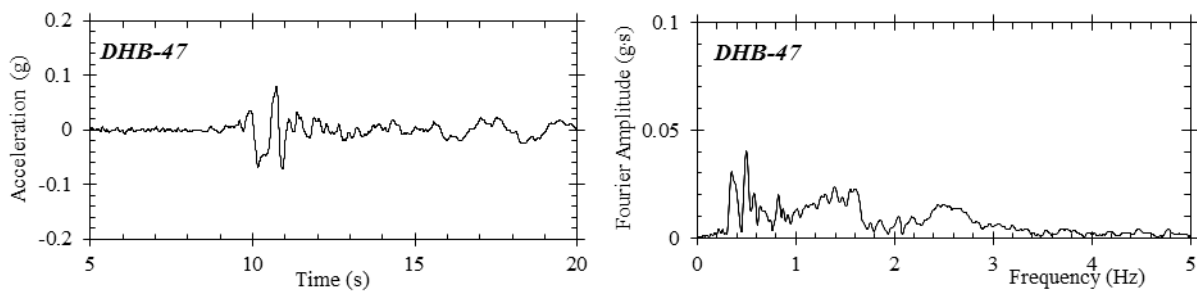


Figure 5. EW component of the acceleration time history and Fourier amplitude spectrum of the DHB-47 seismic signal, assumed as input excitation.

### The Hardening Soil model with small strain stiffness: formulation and calibration

The Hardening Soil model with Small-strain Stiffness (HSsmall) is a combination of the Hardening Soil (HS) model proposed by Schanz et al. (1999) and the elastic small-strain overlay model, developed by Benz et al. (2009). The HSsmall model allows to describe the hysteretic para-elastic behaviour of soil at very small strain, by introducing the initial shear stiffness modulus  $G_0$  and the evolution of the secant shear stiffness ratio  $G_s/G_0$  with shear strain.

A basic feature of the model is the dependency of the soil stiffness on the stress level, which is implemented by a function of the effective stress and strength parameters  $c'$  and  $\phi'$ :

$$G_0 = G_0^{ref} \left( \frac{c' \cos \varphi' + \sigma'_3 \sin \varphi'}{c' \cos \varphi' + p'^{ref} \sin \varphi'} \right)^m \quad (1)$$

where  $G_0^{ref}$  is the reference initial shear modulus corresponding to the reference confining pressure  $p'^{ref}$  (assumed equal to 100 kPa),  $m$  is a constant that depends on soil type and  $\sigma'_3$  is the minor principal effective stress.

The modulus reduction curve is implemented as a modified version of the simple hyperbolic law proposed by Hardin and Drnevich (1972):

$$\frac{G_s}{G_0} = \frac{1}{1 + 0.385 \left| \frac{\gamma}{\gamma_{0.7}} \right|} \quad (2)$$

where  $\gamma_{0.7}$  is the deformation at which the secant shear modulus is reduced to about 70% of  $G_0$ .

The hysteretic behaviour in unloading-reloading is formulated by the Masing's rules: under cyclic loading conditions, a hysteresis loop is described, giving a measure of energy dissipation (Brinkgreve et al., 2007).

The derivative of Eq. (2) with respect to the shear strain provides the expression for the tangent shear stiffness modulus  $G_t$ , which is limited by a lower cut-off value. When the strain level reaches the limit  $\gamma_{cut-off}$  (Eq. 3), the tangent shear stiffness modulus  $G_t$  becomes constant and equal to the unloading-reloading shear stiffness modulus  $G_{ur} = E_{ur}/2(1+\nu_{ur})$

$$\gamma_{cut-off} = \frac{\gamma_{0.7}}{0.385} \left( \sqrt{\frac{G_0^{ref}}{G_{ur}^{ref}}} - 1 \right) \quad (3)$$

Similar expressions to Eq. (1) are introduced in the model for the definition of the dependency on the state of stress of the unloading-reloading modulus  $E_{ur}$ , the secant stiffness in standard drained triaxial test  $E_{50}$  and the tangent stiffness for primary oedometer loading  $E_{oed}$ .

The HSsmall model is an isotropic hardening elasto-plastic model, characterized by two yield surfaces: a shear hardening yield surface, resembling the hyperbolic law, and a cap yield surface, introduced to delimit the elastic region for compressive stress paths. The former yield surface is a function of the deviatoric plastic strain and it can expand up to the Mohr-Coulomb failure criterion, with a non-associated flow rule; the cap yield surface is governed by plastic volumetric strain and an associated flow rule is employed.

Model calibration is carried out with reference to the available data and a summary of the model parameters for each layer is provided in Table 1. The reference initial shear stiffness modulus  $G_0^{ref}$  and the parameter  $m$  are selected to obtain the best fitting with the shear wave velocity profile provided by a cross-hole test (Figure 3b). The shear strain level  $\gamma_{0.7}$  is calibrated using the decay curves of shear modulus and damping ratio (Figure 4). Because of the dependence of  $\gamma_{cut-off}$  on the ratio  $G_0^{ref}/G_{ur}^{ref}$ , this latter is kept low in order to provide a realistic amount of damping ratio at relatively large strain level. The unloading-reloading stiffness modulus  $G_{ur}^{ref}$  is set equal to  $G_0^{ref}/4$  for the silty sand layer, while for sand with gravel and silty clay layers a ratio of  $G_0^{ref}/2.5$  is considered suitable. The other stiffness parameters,  $E_{50}^{ref}$  and  $E_{oed}^{ref}$ , are assumed as three times lower than the elastic unloading-reloading Young's modulus  $E_{ur}^{ref}$ , which is evaluated from  $G_{ur}^{ref}$  adopting the Poisson's ratio  $\nu_{ur}$ . For coarse-grained soils, the Poisson's ratio is assumed equal to 0.3, accordingly to the experimental observations by Jiang et al. (1997), while it is considered equal to 0.25 for the silty soil layers.

The earth pressure at rest coefficient,  $K_0$ , is estimated according to the Jaky's expression for coarse-grained soils and according to the expression valid for overconsolidated soil  $K_0^{oc} = (1 - \sin \varphi') OCR^{0.5}$  for fine-grained layers.

For the sand with gravel and silty sand layers, the overconsolidation ratio OCR is fictitiously set to 10 in order to exclude yielding during radial compressive stress paths.

Table 1. HSsmall model parameters used in FE analyses

	Silty sand (0-17 m)	Sand with gravel (17-23 m)	Silty clay (23-29 m)	Sand with gravel (29-36 m)	Silty clay (36-47 m)
$c'$ (kPa)	0	0	10	0	10
$\varphi'$ (°)	30	35	24	37	24
OCR (-)	10	10	5	10	5
$K_0^{nc}$ (-)	0.5	0.4264	0.5933	0.3982	0.5933
$K_0^{oc}$ (-)	-	-	1.327	-	1.327
$G_0^{ref}$ (MPa)	90	115	65	160	65
$\gamma_{0.7}$ (%)	0.011	0.01	0.025	0.011	0.025
$m$ (-)	0.54	0	0.42	0	0.42
$\nu_{ur}$ (-)	0.3	0.3	0.25	0.3	0.25
$E_{ur}^{ref}$ (MPa)	60	119.5	65	164.5	65
$E_{s0}^{ref}$ (MPa)	20	39.83	21.67	54.81	21.67

According to its formulation, the HSsmall model provides almost null values of damping ratio at very small-strain level; in order to introduce a small amount of damping, viscous damping is added by means of the Rayleigh formulation, which is characterised by a damping matrix expressed as a linear combination of the mass and stiffness matrices

$$[C] = \alpha_R [M] + \beta_R [K] \quad (4)$$

where  $\alpha_R$  and  $\beta_R$  are frequency-dependent coefficients, expressed by

$$\begin{Bmatrix} \alpha_R \\ \beta_R \end{Bmatrix} = \frac{2D^*}{\omega_m + \omega_n} \begin{Bmatrix} \omega_m \omega_n \\ 1 \end{Bmatrix} \quad (5)$$

$D^*$  is the target damping ratio, here assumed equal to 1%;  $\omega_m$  and  $\omega_n$  are the angular frequencies selected according to the calibration procedure proposed by Amorosi et al. (2010). The calibration required a preliminary equivalent linear analysis, performed by the code EERA (Bardet et al., 2000), in order to define the amplification function with reference to the EW seismic acceleration component. Based on that, the first control frequency  $f_m$  is identified as the fundamental frequency of the soil deposit ( $f_m = 1$  Hz), while the second control frequency  $f_n$  is the frequency where the amplification function becomes lower than one ( $f_n = 3.5$  Hz).

### Numerical models

The free-field ground response analysis and the dynamic SSI analysis are performed in the time domain, applying the EW horizontal components of the seismic event LSST7. The bedrock was assumed at the depth of 47 m below the ground surface, where the recorded DHB-47 time history was applied as input motion.

The geometrical model adopted for the free-field seismic ground response analysis consists in a 47 m thick soil column of width 10 m x 10 m (Figure 6a). The soil domain is discretised by 5329 10-noded tetrahedral elements.

When the structure is included, the 47 m thick geometrical model consists in a soil domain of width equal to 70 m x 70 m. In this analysis the nuclear power plant containment structure is

modelled as a cylindrical *plate* structure of 0.305 m thickness (the outer diameter is 10.52 m) with two flat circular *plate* elements at the roof and the bottom characterised by 1.07 and 0.91 m thickness, respectively (Figure 6b). The structure is embedded at the depth of 4.6 m below the ground surface. These elements are modelled as linear visco-elastic concrete materials with unit weight of 25 kN/m<sup>3</sup>, Young's modulus  $E = 2.53 \cdot 10^4$  MPa and Poisson's ratio  $\nu = 0.2$ . Due to the lack of direct information, a damping ratio of 5 % (typical for concrete material structures) is assumed and included by means of the Rayleigh formulation, selecting control frequencies of 1 Hz and 10 Hz.

The steam generator prototype is modelled as a Single-Degree Of Freedom (SDOF) structure, whose fixed-base natural frequencies are 5.4 Hz and 5 Hz respectively in EW and NS directions (EPRI, 1991). The SDOF model is characterized by a concentrated mass connected to the containment structure through a weightless beam element column. The unit weight of the mass, modelled as a plate element of unit dimensions, is 52.46 kN/m<sup>3</sup>, while the rectangular cross-section of the beam has the following dimensions: 0.452 and 0.419 m, respectively along the EW and NS directions (Figure 6c). A damping ratio of 1.5% is introduced for the element column by means of the simplified Rayleigh formulation, selecting a control frequency of 5 Hz.

In both numerical models the soil deposit is divided into 47 layers of unit thickness in the vertical direction, in order to satisfy the condition that the size of the finite element must be smaller than about one/eighth of the wavelength associated with the maximum frequency component  $f_{max}$  of the input wave (equal to 10 Hz). The boundary conditions adopted in the pre-seismic static stages are characterised by total fixities for nodes at the bottom of the mesh, while horizontal displacements are constrained for the nodes located on the vertical sides of the soil domain. In the dynamic phase, "tied nodes" boundary condition are introduced. This condition is obtained introducing horizontal node-to-node anchors elements, characterized by high values of axial stiffness  $EA$  (equal to 10<sup>9</sup> kN). In order to restore the stress equilibrium perturbed by the modification of the horizontal constraints introduced switching from the static to the dynamic phase, pressures corresponding to lithostatic distribution of horizontal effective stresses are introduced on the vertical sides of the mesh.

All dynamic analyses are performed under undrained conditions.

For time integration scheme, the Generalized Newmark method is employed, with Newmark parameters  $\beta_1$  and  $\beta_2$  respectively equal to 0.6 and 0.605, ensuring the algorithm to be unconditionally stable.

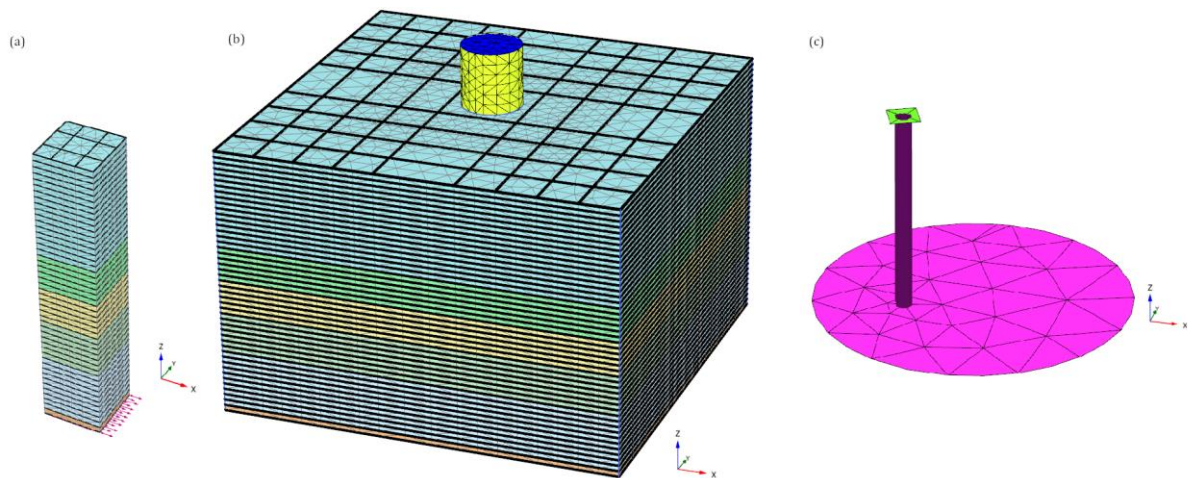


Figure 6. Numerical models implemented in the seismic ground response analyses (a) and in the SSI interaction analyses (b). SDOF model representative of steam generator structure (c)

**Non-linear ground response analysis**

The acceleration time histories predicted by the non-linear analyses are compared to the motion recorded at ground surface (FA1-5) and at the depth of 17 m (DHB-17). Comparisons are provided in Figure 7 in terms of acceleration time histories, Fourier amplitude spectra and acceleration response spectra.

The time domain numerical simulation leads to signals that are in fair agreement with those recorded at the same depths. Only a slight over-prediction of the peak acceleration is observed at the ground surface, while zero crossings are well predicted by the numerical analysis. The comparison in terms of response spectra improves at larger depth (DHB-17), where a slight over-prediction of the spectral acceleration is only observed in the range of periods between 0.15 s and 0.3 s.

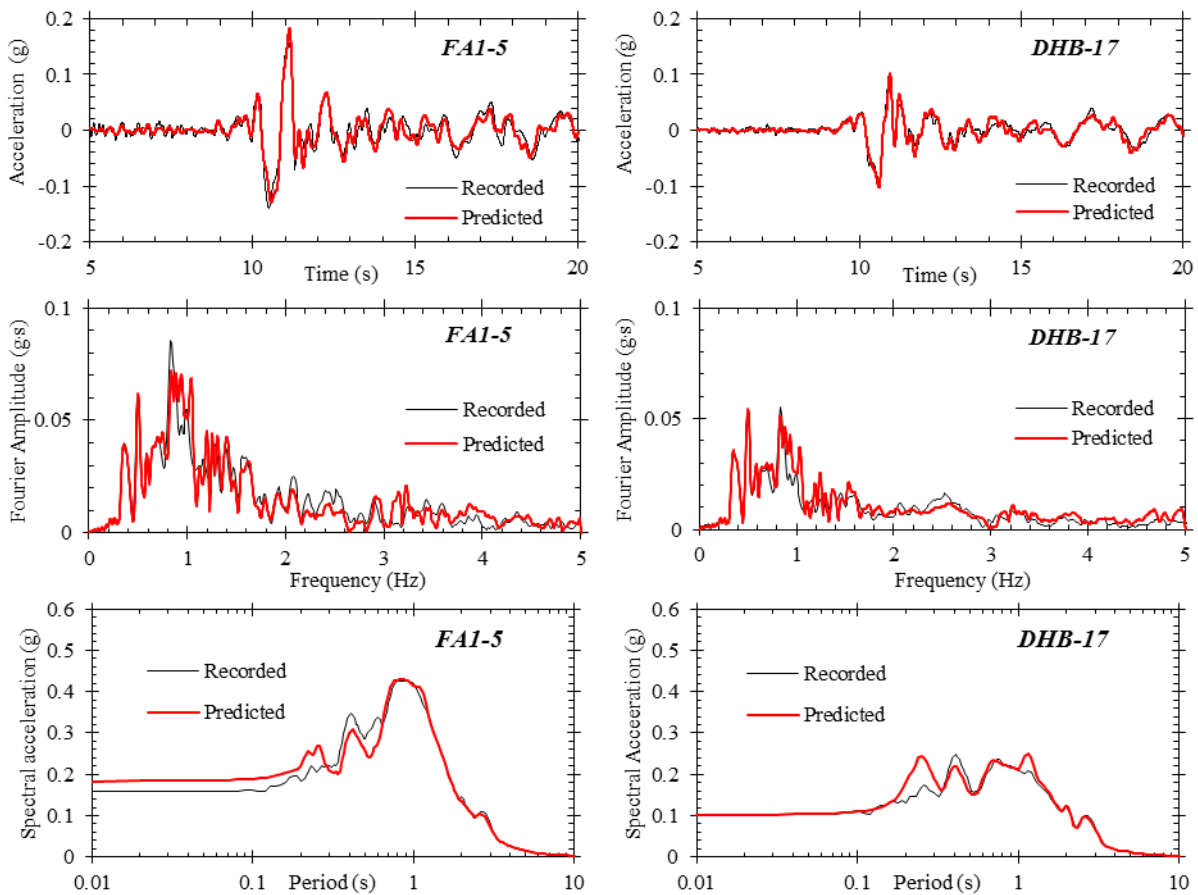


Figure 7. Comparison between computed and recorded motion at the ground surface and at the depth of 17 m in terms of acceleration time histories, Fourier amplitude spectra and elastic response spectra.

**Dynamic soil-structure interaction of 1/4-scale nuclear power plant**

The numerical dynamic response of the 1/4-scale containment structure is compared to the response recorded by the accelerometer F4US, located on the roof, and accelerometer F4LS, at the base of the model, in terms of acceleration time histories, Fourier amplitude spectra and response spectra (Figure 8).

The acceleration time history predicted at the bottom of the containment structure matches well that recorded at F4LS, both in terms of peak acceleration and zero crossings. The good prediction is confirmed by the elastic response spectra as well as Fourier amplitude spectra, this latter showing a slight over-damping of Fourier amplitude at about 0.50 and 0.85 Hz. The dynamic response predicted at the top of the structure (F4US) is characterised by a general underestimation of the acceleration amplitudes, even though the peak one is nicely

reproduced. Correspondingly, Fourier amplitudes are over-damped in the frequency range between 0.5 Hz and 3 Hz (as in the range of periods 0.3 s and 2 s in the response spectra). This should be related to the possibly incorrect selection of the damping ratio for the structural model: better predictions would have been obtained if specific experimental data were available with reference to 1/4-scale containment structure model.

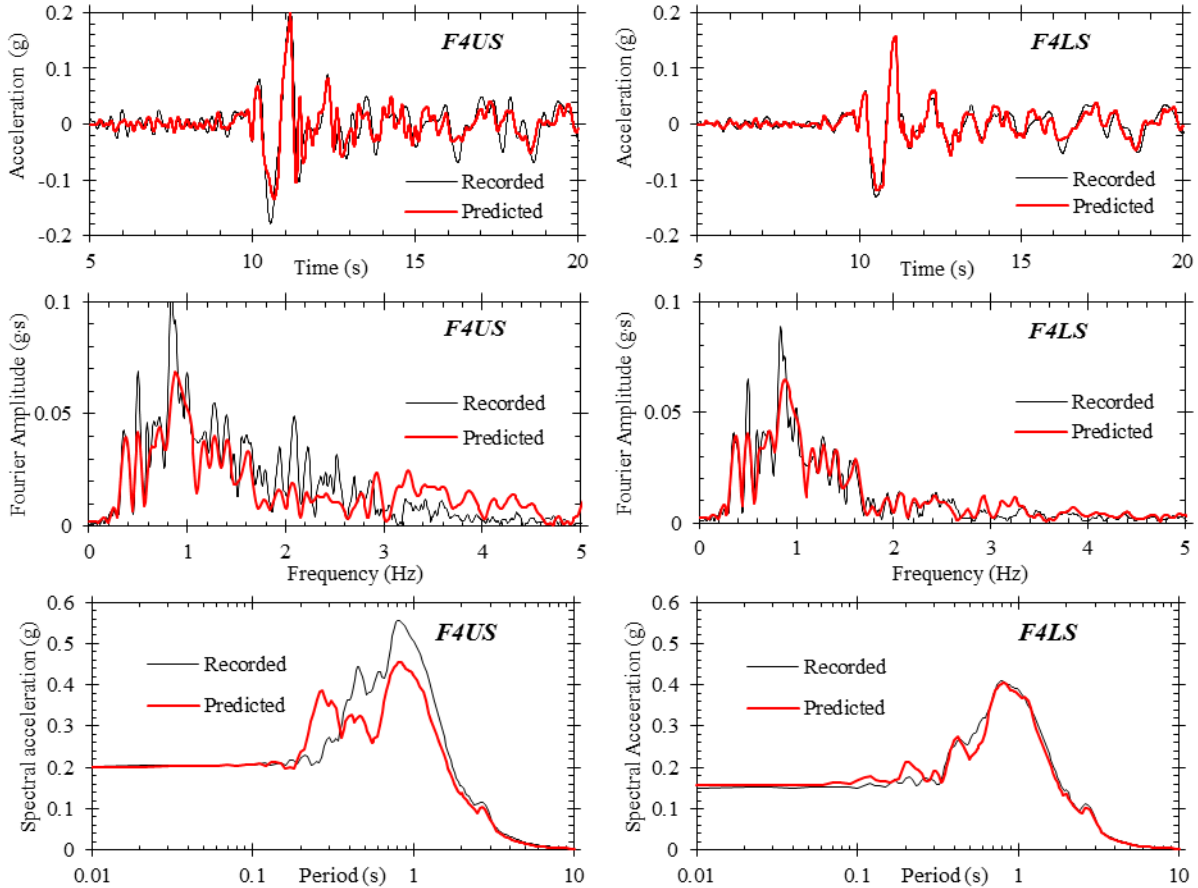


Figure 8. Comparison between computed and recorded motion on the roof (F4US) and on the base (F4LS) of the 1/4-scale model of containment structure in terms of acceleration time histories, Fourier amplitude spectra and elastic response spectra.

### Conclusions

A 3D numerical approach is proposed in the paper to back-analyse the free-field seismic ground response and the soil-structure interacting response of a small-scale structure whose behaviour was recorded during the LSST7 event in Lotung, Taiwan. The soil behaviour was simulated by the advanced constitutive model HSsmall, while a linear visco-elastic hypothesis was assumed for structural model. The calibration of the geotechnical and structural models were performed with reference to the available experimental data and existing research works published in the past on the same case history.

Numerical results prove to be in good agreement with the free-field down-hole measurements at depth and at the ground surface, both in terms of peak acceleration and zero crossings. The main features of the dynamic structural response were also captured by the numerical simulation.

The overall comparison confirms the validity of the proposed numerical approach, which is currently being extended to include multidirectional applications of the seismic actions.

## REFERENCES

- Amorosi A, Boldini D and Elia G (2010) Parametric study on seismic ground response by finite element modelling, *Computers and Geotechnics*, 37 (4): 515-528
- Bardet JP, Ichii K, Lin CH (2000) *EERA: A computer program for equivalent-linear earthquake site response analyses of layered soil deposits*, Department of Civil Engineering, University of Southern California
- Benz T (2006) *Small-strain stiffness of soils and its numerical consequences*, Ph.D. Thesis, Institute für Geotechnik, University of Stuttgart, Germany
- Benz T, Vermeer PA and Schwab R (2009) A small strain overlay model, *International Journal for Numerical and Analytical Methods in Geomechanics*, 33: 25-44
- Borja RI, Chao HY, Montans FJ and Lin CH (1999) Nonlinear ground response at Lotung LSST site, *Journal of Geotechnical and Geoenvironmental Engineering*, 125(3): 187-197
- Borja RI, Chao HY, Montans FJ and Lin CH (2000) Modelling non-linear ground response of non-liquefiable soils, *Earthquake Engineering and Structural Dynamics*, 29: 63-83
- Brinkgreve RBJ, Kappert MH and Bonnier G (2007) *Hysteretic damping in a small-strain stiffness model*, Proceedings of the 10<sup>th</sup> International Symposium on Numerical Models in Geomechanics NUMOG 10, London, 737-742
- De Mello VFB (1971) *The Standard Penetration Test, State of the Art Report*, Proceedings of the 4<sup>th</sup> Panamerican Conference on Soil Mechanics and Foundation Engineering, San Juan, Puerto Rico
- Elgamal AW, Zeghal M, Tang HT and Stepp JC (1995) Lotung downhole array. I: Evaluation of site dynamic properties, *Journal of Geotechnical Engineering*, 121(4): 350-362
- EPRI (1991) *Post-Earthquake analysis and data correlation for the 1/4-scale containment model of the Lotung experiment*. Report No 7305-SL, Electric Power Research Institute, Palo Alto, California.
- EPRI (1992) *Spatial variation of earthquake ground motion for application to Soil-Structure Interaction*. Report No TR-100463, Electric Power Research Institute, Palo Alto, California.
- Kramer SL (1996) *Geotechnical earthquake engineering*, Prentice Hall, Englewood Cliffs, New Jersey
- Jiang GL, Tatsuoka F, Flora A and Koseki J (1997) Inherent and stress-state-induced anisotropy in very small strain stiffness of a sandy gravel, *Geotechnique*, 47 (3): 509-521
- Schanz T, Vermeer PA and Bonnier PG (1999) *The Hardening Soil model: Formulation and Verification*, Beyond 2000 in Computational Geotechnics, Balkema, Rotterdam, 281-296
- Veletsos AS and Nair VV (1975) Seismic interaction of structures on hysteretic foundations, *ASCE Journal of Structural Division*, 101: 109-129
- Vucetic M and Dobry R (1991) Effect of soil plasticity on cyclic response, *Journal of Geotechnical Engineering*, 117: 89-107
- Wolf JP (1985) *Dynamic soil-structure interaction*, Prentice Hall, Englewood Cliffs, New Jersey
- Zeghal M, Elgamal AW, Tang HT and Stepp JC (1995) Lotung downhole array. II: Evaluation of soil nonlinear properties, *Journal of geotechnical engineering*, 121(4): 363-378